Highly Sensitive Indirect Time-of-Flight Distance Sensor With Integrated Single-Photon Avalanche Diode in 0.35 μm CMOS

Alexander Kuttner, *Graduate Student Member, IEEE*, Michael Hauser, *Graduate Student Member, IEEE*, Horst Zimmermann, *Senior Member, IEEE*, and Michael Hofbauer, *Member, IEEE*

***Abstract*—This work describes the architecture and measured capabilities of an optical distance sensing application specific integrated circuit (ASIC) manufactured in 0.35 μm CMOS with a nominal supply voltage of 3.3 V for indirect time-of-flight. An integrated single-photon avalanche diode (SPAD) with an active diameter of 38 μm is used as detector with 6.6 V excess bias, active quenching and active resetting circuit. Phase measurement is performed using a digital correlation approach with digital counters. Due to the unmatched sensitivity of SPADs, sub-cm accuracy measurements can be performed with a received signal power in the pW range. Background light ratios up to 24.1 dB still allow sub-cm precision. Depending on the required accuracy and the received optical power, the measurement time can be adjusted freely up to several seconds only limited by digital counter depth. Compared to a pin-photodiode iTOF sensor in the same technology, this chip has a sensitivity improvement of 33.3 dB and 40.7 dB for a distance accuracy of 1 cm and 10 cm, respectively, while reducing the effective measurement time by 75% at the same time. The chip size is 1.4 mm $\times$ 1.4 mm including two correlator blocks, for simultaneous acquisition of two phase steps. The number of correlators is scalable allowing parallel measurements of phase correlations.**

***Index Terms*—Sensors, electro-optical systems, SPAD, indirect time of flight, cw-iTOF, correlation, CMOS, active quenching.**

I. Introduction

OPTICAL distance measurement has become of increasing importance in various fields of applications such as object detection in autonomous driving, security or consumer electronics. Using single-photon avalanche diodes (SPADs) allows to considerably reduce the required amount of optical power due to their high sensitivity. This allows measuring longer distances than using regular photodiodes.

In direct time-of-flight (dTOF) the traveling time of a light pulse from a light source to an object and back to the detector is measured. To achieve high precision, very accurate time-to-digital converters are required. E.g., for 1 cm of distance measurement precision the required time-measurement precision corresponds to ~66.7 ps.

Manuscript received May 17, 2022; revised June 1, 2022; accepted June 7, 2022. Date of publication June 13, 2022; date of current version June 21, 2022. This work was supported by the Austrian Science Fund under Grant P30927-N30. *(Corresponding author: Alexander Kuttner.)*

The authors are with the Institute of Electrodynamics, Microwave and Circuit Engineering, Technische Universität Wien, 1040 Vienna, Austria (e-mail: alexander.kuttner@tuwien.ac.at; michael.hauser@tuwien.ac.at; horst.zimmermann@tuwien.ac.at; michael.hofbauer@tuwien.ac.at).

Digital Object Identifier 10.1109/JPHOT.2022.3182153

In contrast to this, indirect time of flight (iTOF) uses a continuous modulated light signal. The round trip introduces a phase shift that correlates to the distance of the object [1].

In this work, a continuous wave (CW) iTOF measurement technique with a square-wave modulated light source is used. From the measured phase shift $\Delta\varphi$ the distance d of the object can be calculated by [2]:

$$d = \frac{c_0}{2f_{mod}} \frac{\Delta\varphi}{2\pi}, \tag{1}$$

where c_0 is the speed of light and f_{mod} is the modulation frequency of the CW modulated light signal. To increase the accuracy of the measurement either $\Delta\varphi$ has to be measured more exactly or the modulation frequency has to be increased.

A disadvantage of this method is that a phase wrap cannot be detected during a single measurement. The measurable distance, also called unambiguous range, depends on the modulation frequency and can be calculated by:

$$d_{\max} = \frac{c_0}{2f_{mod}}, \tag{2}$$

It is possible though to perform two or more measurements with different modulation frequencies to considerably increase the unambiguous range.

The phase of the received square-wave modulated light is calculated by cross correlation in this work. Cross correlation of two square-wave signals phase shifted by $\Delta\varphi$ results in a triangle shifted by $\Delta\varphi$. Within this work, Fast Fourier Transformation (FFT) is used to calculate the phase of the fundamental wave of this triangle, which is the sought phase shift $\Delta\varphi$. This cross correlation is performed by calculating the correlation of the measured light signal with the modulation signal of the laser and phase shifted copies of it.

A multiphase continuous wave modulation iTOF approach in the same 0.35 μm CMOS technology, has already been presented in [2] using pin-diodes and an analog charge integrator instead of SPADs. With a modulation frequency of 12.5 MHz, a standard deviation of the measured distance of 1 cm has been reached with 1 nW of signal power. The background light was rejected up to a factor of 600.

In this paper, we compare this approach, with our iTOF SPAD approach using a SPAD as detector, in order to investigate the possible gain in sensitivity, if the same measurement approach,

as well as the same technology is used. We show that the achievable improvement is remarkable. This is explained first by the improved sensitivity of the SPAD itself, and second by the higher possible modulation frequency.

In [3], an iTOF approach is used with a 64 × 32 SPAD array in 0.35 μm, achieving a precision of 2.8 cm with 30 MHz correlation frequency, 4 phases and 45 ms integration time. The used SPADs reach a photon detection probability (PDP) of 45% at 410 nm. In [4], a continuous wave iTOF method is used with an all-digital phase domain delta sigma loop for a 128 × 96 SPAD sensor. A precision of up to 2.5 cm is reached with a modulation frequency of 3.33 MHz. The used 8 μm diameter SPADs have a dark count rate (DCR) of 100 cps. In [5], a dTOF 32 × 128 SPAD image sensor in a 0.35 μm technology is presented, the used time-to-digital converters (TDC) reach a timing resolution of 78 ps and a measurement precision of under 2 cm. The used SPADs have a median DCR of 22.7 kHz. In [6], a 64 × 64 SPAD flash LIDAR sensor in 130 nm HV CMOS with a combination of TDCs and triple integration interpolators is used to reach a timing resolution of 13 ps, corresponding to a depth resolution of 1.95 mm. In [7], a 64 × 64 iTOF SPAD sensor array in a 110 nm technology is presented, using analog pulse counters that achieves a precision of down to 1.35 cm with a fill factor (FF) of 26.3% and a DCR of 100 cps. A modulation frequency of up to 50 MHz is used. In [8], a 400 × 10 dTOF SPAD array achieves a precision of 2.3 mm. Self-configurable routing is used to share the TDCs among the SPADs. The maximum measurable distance is 2 m. A 189 × 600 back-illuminated SPAD array for automotive applications with a range of up to 200 m and a depth accuracy of 15cm is presented in [9]. They use 3D stacking, using different processes to create the SPADs and electronics and connecting the dies, to increase the FF. However, this increases the complexity of the design. In [10], an all-in-one 8 × 8 SPAD distance sensor is presented including electronics to drive the required laser. The device works up to a distance of 4 m with an error of less than 5%.

However, a comparison of the sensitivities of these sensors is difficult, since the sensitivity of the sensor itself was not evaluated in these papers, rather the performance of the sensor with an optical system. Therefore, our work puts an emphasis on the comparison with the pin iTOF sensor of [2], which is built in the same technology, also uses iTOF, and also characterizes the sensor's sensitivity, to show the increase in sensitivity and precision when using a SPAD instead of a pin diode.

In Section II, the architecture and design of the presented iTOF sensor chip will be discussed. In Section III, the measurement setup used for optoelectronic ASIC characterization is presented. Section IV presents and discusses iTOF measurement results. Section V concludes these findings.

II. Design

The sensor was fabricated in a 0.35 μm 2P4M CMOS process with an epitaxial p- layer for pin diodes. Fig. 1 shows the chip photo.

The ASIC was designed using Cadence software suite in an analog-on-top approach. While the SPAD, AQC, and clock

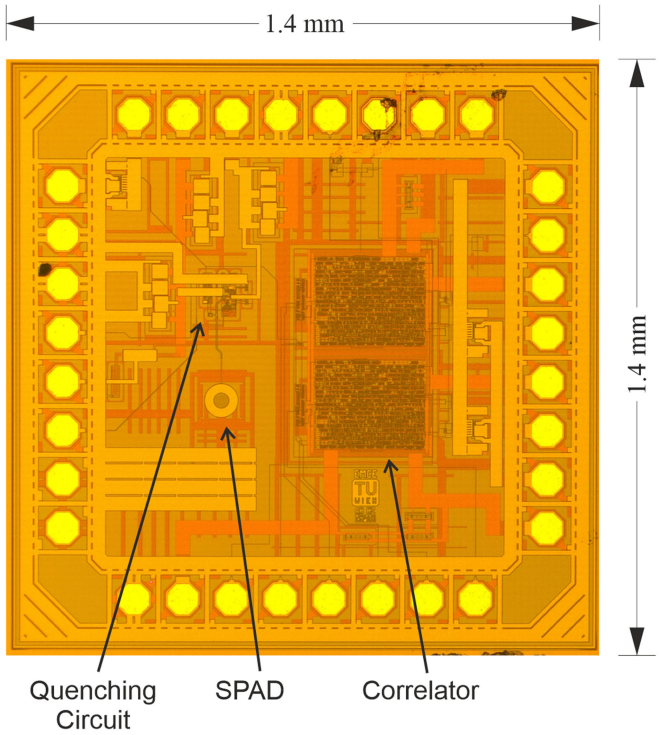

Fig. 1. Photo of the fabricated ASIC.

generation circuit are full-custom analog designs, the correlator blocks including readout are created using digital synthesis from VHDL code. Fig. 2 shows the block diagram of the ASIC. As for the quencher and fully integrated pin-SPAD, proven designs presented in [11] and [12] were used with some improvements of the SPAD regarding size and edge breakdown protection. The pin-SPAD has an active area diameter of 38 μm and a breakdown voltage of 33.5 V. The active-quenching active-resetting circuit (AQC) with up to 6.6 V of excess voltage has an adjustable deadtime between 9.7 ns and 45 ns with adjustable reference voltage (avalanche detection threshold). The size of the quenching circuit is 130 μm × 130 μm.

A block diagram of the correlator block is depicted in the top part of Fig. 2. Due to the digital nature of the AQCs' output, a fully digital correlator design can be used, contrary to the approach in [2] using a pin photodiode. Digital binary correlation is performed using an up/down counter. Each correlator block consists of an 8-bit up, 8-bit down and a 20-bit carry counter, resulting in 28 bits in total. The bit-depth was chosen to allow long correlation measurements and low correlation frequencies. This allows a correlation time of 2.68 s even if the output of the quencher saturates in one counting direction and shows zero counts in the other one, assuming the shortest possible dead time (i.e., 9.7 ns) is selected. When the SPAD is not in saturation, even longer measurement times are possible. If for a specific application, chip area is more critical than very long integration times, scaling the counter size down is possible and reduces required chip area approximately linearly to the number of bits. When the readout procedure is started, the combined value is calculated and stored in a shift register.

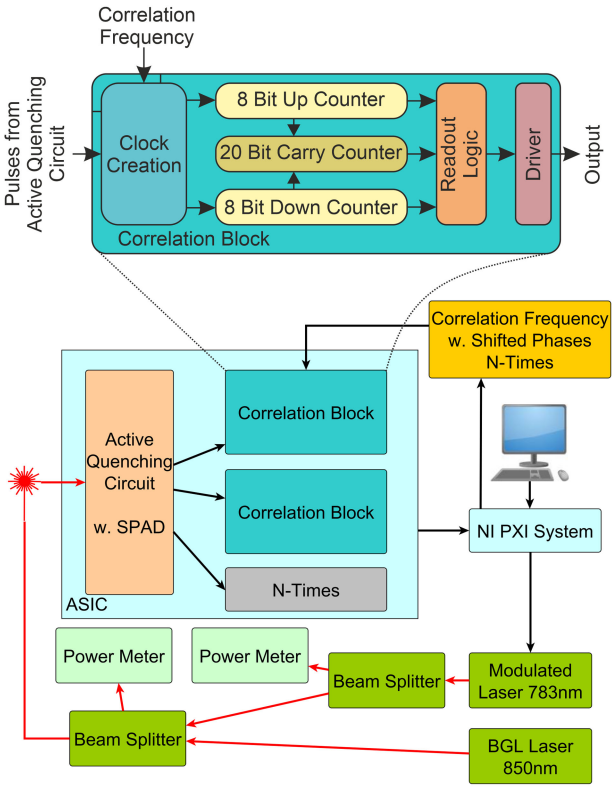

Fig. 2. Block diagram of ASIC with measurement setup.

While the counters are designed to work with a synchronous clock, the clock creation circuit, which decides if a photon-generated pulse is an up or down count, is designed asynchronously, since the pulses created by the quenching circuit are not synchronized with the clock domain of the modulation frequency.

First, the pulse created by the quencher is shortened to a specific length. The modulation signal is used to gate those pulses to pulse generators that drive the clock trees of the digital circuitry. The path of the coarse counter clock is designed to be faster than the clocks for the fine counters to prevent hold violations.

In iTOF, many SPAD induced non-idealities do not have a significant impact on the resulting accuracy. E.g. dark counts cancel each other out to a large extent because in average they occur in the same number during up and down counting phases. The SPADs avalanche propagation time as well as the afterpulsing probability leads to an offset in the measured distance and therefore the sensor has to be calibrated. The jitter of the avalanche propagation cancels itself out but leads to a loss of photons usable for the measurement and in addition limits the maximum achievable precision, even for long correlation times.

III. Measurement Setup

A block diagram of the measurement setup is depicted in Fig. 2. The device under test (DUT) is not packaged but directly mounted and bonded as chip on a printed circuit board (PCB). It is placed in a dark box, including a thermally stabilized mounting block. A 783 nm externally modulated single mode fiber laser with an optical attenuator is used to provide the signal for measurement. To emulate background light (BGL), a second continuous wave (cw) operated laser at a different wavelength λ (850 nm is used). This light generates pulses in the SPAD and quencher, which are uncorrelated to the modulated laser light. The wavelength of the light emulating the BGL is not important, as long as it is not correlated to the modulated laser light and as long as it is detectable by silicon detectors. The signals are combined and led into the dark box where a fiber can be adjusted above the active area of the chip using a motorized xyz-stage. The used single-mode fiber SM800 has a mode field diameter of $\sim$5 μm, which is considerably smaller than the active area of the SPAD, guaranteeing, that all of the light is coupled into the SPAD. Using beam splitters and optical power meters for monitoring both lasers, we know the amount of optical power within the fiber. This is crucial for determining the sensitivity of the detector.

The measurements are performed using a National Instruments PXI system including the Flex RIO FPGA NI PXIE-7962R together with the digital I/O adapter module NI-6587 for generating all the control and modulation signals and for reading out the sensor. This setup allows automated measurements covering many degrees of freedom, to enable in-depth ASIC characterization. This measurement approach was chosen to characterize the standalone ASIC, without the impact of an optical system, allowing to evaluate the sensitivity given by the sensor itself.

For each operating point, 100 correlation triangles with 8 phase steps were recorded and the standard deviation of the measured distance was calculated as a measure of precision. For longer measurements (100 ms and 1 s integration time per phase step) only 25 triangles were recorded in order to limit the required measurement time. The current design allows performing two phase steps at a time; due to the scalable nature of the design, it would be possible in principle to perform all phase steps at once when using more correlator blocks on the ASIC, while still being able to use only one SPAD and quencher. There is, however, of course a trade-off with the required chip area. However, measuring two phase steps at a time, is already an advantage compared to the pin iTOF approach in [2], where due to the analog nature of the detection process, only one phase step could be detected at a time. A modulation frequency of 62.5 MHz was used for these measurements. Also, this is already considerably better than what was possible in [2], where a modulation frequency of only 12.5 MHz was used.

IV. Measurement Results and Discussion

Regarding the SPAD induced non-idealities, the measured DCR and afterpulsing probability (APP) are shown in Fig. 3. In the usable range of excess voltage V_{excess} (up to 6.6 V) the DCR reaches 71 kcps and the APP goes up to 13.7%, for a dead time of 10 ns. These rather high numbers result from the large sensitive volume of the used pin-SPAD structure realized in this process. In principle it would have been possible to pre-select an ASIC with a SPAD showing lower DCR and APP. However, due to the

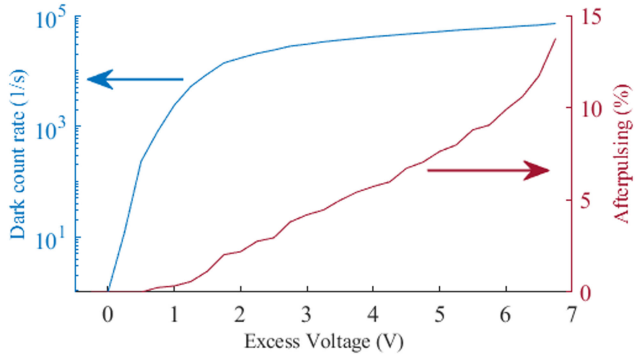

Fig. 3. Measured dark count rate and afterpulsing probability of the used SPAD and AQC.

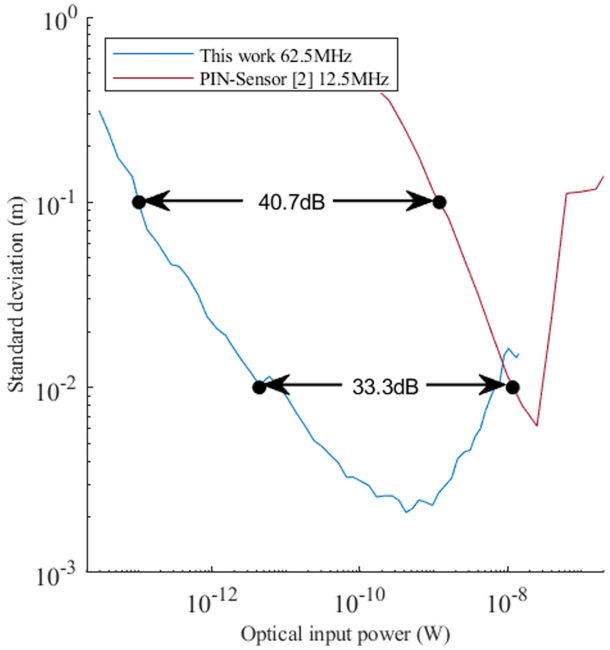

Fig. 4. Standard deviation versus optical input power for 100μs phase step integration time.

correlating nature of this measurement approach, DCR and APP have only a very negligible influence on the system performance. This thick SPAD features a high PDP even for near-IR light, at 782 nm the PDP achieved with this structure in this process is 31% for $V_{excess} = 6.6$ V [12].

Fig. 4 shows a distance measurement for an integration time of 100 μs per phase step. In [2], 16 phase steps were used for multiphase correlation, while in this work we use only 8, so the total measurement time (e.g., 800 μs in this case) is already halved. Considering that in our approach two phase steps are measured at a time, reduces the effective measurement time by another factor of two compared to [2], resulting in a total reduction by 75%. The results from [2] are included into the diagram for comparison. Although, we were able to decrease the measurement time by 75%, using a SPAD increases the sensitivity considerably. This improvement is 33.3 dB and 40.7 dB for standard deviations of 1 cm and 10 cm, respectively.

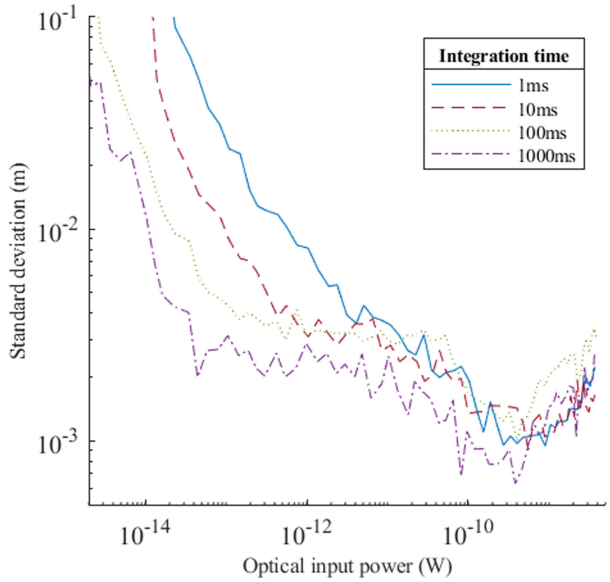

Fig. 5. Measurement precision versus optical input power for different measurement times.

Consequently, this sensitivity improvement, allows either to reduce the optical power of the light source by more than 30dB for the SPAD iTOF sensor compared to the pin iTOF sensor, or if the same optical power is used, to use the SPAD iTOF sensor for much longer distances (i.e., more than 30 times further, according to Eq. 3) compared to the pin iTOF sensor, without losing sensitivity.

To give an indication of the achievable distances using a laser with just 1 mW of optical power, the following estimation is presented. With given parameters the used power of the transmitted measurement laser $P_{opt,tra}$, the diameter of the sensor lens d_{lens}, the measured distance d_{meas}, and the reflectivity of the target ρ_0 the impact of an optical system on the received power $P_{opt,rec}$ can be calculated by [13]:

$$P_{opt,rec} = P_{opt,tra} \frac{d_{lens}^2 \pi}{4\pi d_{meas}^2} \rho_0, \tag{3}$$

E.g., for an eye safe optical power of $P_{opt,tra} = 1$ mW, a lens diameter of $d_{lens} = 2.54$ cm, a distance of $d_{meas} = 127$ m and a reflectivity $\rho_0 = 10\%$, 1 pW is received.

With our approach we are measuring the optical length of the fiber with a defined and continuously measured optical power. Influences such as fluctuations of background light or others can be ruled out in that way when measuring the standard deviation of the distance measurement result.

The impact of integration time per phase step on precision can be seen in Fig. 5. For higher optical input powers, a lower bound of precision can be seen that is the same for short and long integration times. For longer integration times, a similar precision can be reached with lower optical input power. For an integration time of 10 ms per phase step, an optical dynamic range (DR) of required input power for sub-cm precision measurements of 35.5 dB is reached. When the measurement time is increased to 100 ms, the optical DR for sub-cm precision is increased to

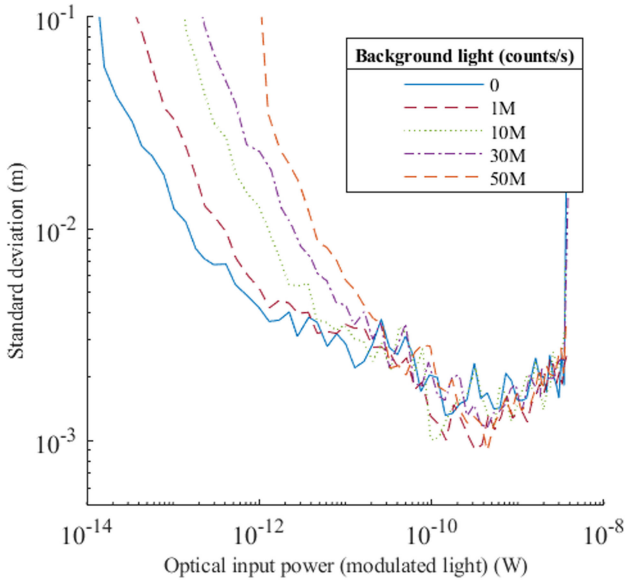

Fig. 6. Standard deviation of measured distance versus optical input power for different background light intensities for 10 ms of integration time.

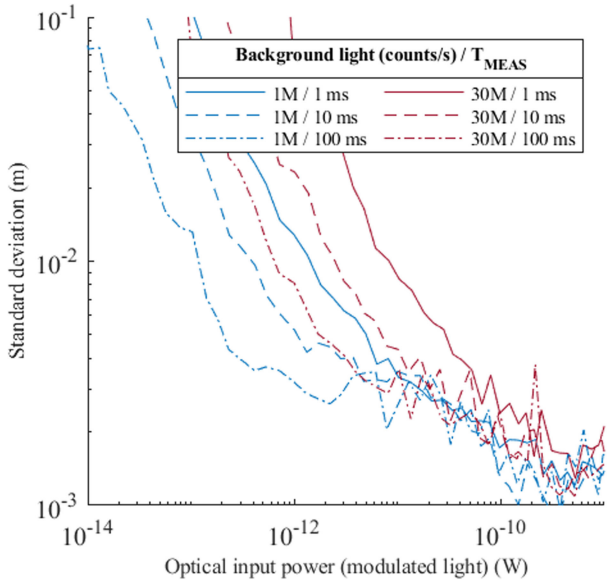

Fig. 7. Measured precision versus optical input power for multiple integration times and two levels of BGL.

41.7 dB. For long integration time, a distance precision even in the sub-mm range is achieved.

With the proposed 28-bit counter, correlation times of 2.8 s are possible, assuming a saturated SPAD output. In contrast to this, [2] only allows a maximum integration time per phase step of slightly under a millisecond. For the measurement and results presented in Fig. 4, for an integration time of 100 μs our sensor shows an optical DR for sub-cm precision of 33.3 dB while [2] only shows an optical DR of 4.4 dB.

Fig. 6 shows the impact of BGL on the measurement for an integration time per phase step of 10 ms. Depending on integration time, BGL suppression still allows sub-cm precision for a ratio of 15.2 dB and 24.1 dB of pulses generated by BGL compared to signal pulses, for 10 ms and 100 ms, respectively.

While BGL degrades the precision of the measurement, this effect can be compensated by using longer integration times as shown in Fig. 7. The pin-sensor presented in [2] shows BGL suppression of 28.0 dB for 20 ms of measurement time but achieves only a precision of 5 cm. This effect can be explained by the saturation effects occurring for SPADs. When using the sensor in an optical system, a narrowband optical filter can be used to further decrease the influence of BGL.

In Table I, the key parameters of the detector of this work are summarized in comparison with the ones of the pin-based detector in the same technology, highlighting the improvement in sensitivity.

Table II compares our work with other state-of-the-art SPAD TOF sensors, showing especially our improvement in distance precision. While our presented work can be compared with the referenced SPAD sensors [3]–[10] in terms of precision, it is not possible to compare them in terms of sensitivity, since the sensitivity of these sensors was not presented. It has to be noted though that by reaching even sub-mm precision better measurement precisions are reached even though utilizing a

TABLE I
COMPARISON SPAD AND PIN iTOF

	This work (SPAD)	[2] (PIN)
Technology	0.35 µm	0.35 µm
Optical device	SPAD	PIN-diode
Core size	340 µm × 250 µm	45 µm × 30 µm
Diode size	38 µm + 130^2 µm^{2}AQC	45 µm × 30 µm
Required opt. power *	0.1 pW	1.2 nW
DR opt **	40.7 dB	4.4 dB
BGL suppression	15.2 dB σ= 1cm	28.0 dB σ= 5cm
Max. integration time	2.8 s	<1 ms

*σ = 10 cm and integration time is 100 μs.
**σ = 1 cm integration time is 100 μs.

TABLE II
COMPARISON OF SPAD DISTANCE SENSORS

	Tech. µm	Type	Pixel	λ nm	PDP %	DCR 1/s	FF %	σ mm
This work	0.35	cw-iTOF	1×1	783	31	48k	0.60	1
[3]	0.35	cw-iTOF	64 × 32	410	45	100	3.1	28
[4]	0.13	cw-iTOF	128 × 96	850	5	100	3.2	25
[5]	0.35	dTOF	32 × 128	810		22.7k	-	<20
[6]	0.13	dTOF	64 × 64	532		10.6k	0.66	2
[7]	0.11	cw-iTOF	64 × 64	480	28	33	26.3	14
[8]	0.16	dTOF	400 × 10	670	23	800	14	23
[9]	0.09/ 0.04*	**	189 × 600	905	22	-	*	150
[10] ***	0.04	dTOF	8 × 8	-	-	-	-	<15

*3D stacked ASICs.
**Hybrid.
***All-in-one device.

SPAD with a DCR orders of magnitudes higher than the other iTOF approaches. At the chosen operating point of $V_{excess} = 4$ V for our SPAD a dark count rate of 48k counts is observed, in contrast to the 100 counts documented in [3], [4] and [7].

V. Conclusion

We have shown, that replacing a PIN-photodiode based iTOF sensor by a SPAD based one, both in the same technology, results in an increased sensitivity of 33.3 dB and 40.7 dB for a distance precision of 1 cm and 10 cm, respectively. Due to reducing the number of used phases from 16 to 8, total measurement times could be halved. Considering that two phase steps can be measured at a time with this digital approach, the effective measurement time is even reduced by 75% compared to the PIN photodiode based iTOF approach. The scalable design proposed in this work can decrease it even further. This is achieved, while keeping the background light suppression in a similar range. The optical dynamic range could also be increased by orders of magnitude. In addition, the higher modulation frequency allows even higher measurement precision. Using digital counters allows longer measurement times, resulting in higher precision, at the cost of required chip area. The size of the digital correlator is way bigger than the analog correlator used in [2], but using a smaller technology node would decrease it, which would not decrease the correlator performance due to its digital nature.

References

[1] F. Piron, D. Morrison, M. R. Yuce, and J.-M. Redouté, "A review of single-photon avalanche diode time-of-flight imaging sensor arrays," *IEEE Sensors J.*, vol. 21, no. 11, pp. 12654–12666, Jun. 2021, doi: 10.1109/JSEN.2020.3039362.

[2] M. Davidovic, J. Seiter, M. Hofbauer, W. Gaberl, and H. Zimmermann, "A background light resistant TOF range finder with integrated PIN photodiode in 0.35 μm CMOS," in *Proc. SPIE Videometrics, Range Imag., Appl. XII; Automated Vis. Inspection*, 2013, vol. 8791, pp. 185–190, [Online]. Available: https://doi.org/10.1117/12.2021021

[3] D. Bronzi *et al.*, "100000 frames/s 64 $\times$ 32 single-photon detector array for 2-D imaging and 3-D ranging," *IEEE J. Sel. Topics Quantum Electron.*, vol. 20, no. 6, pp. 355–364, Nov./Dec. 2014, Art no. 3804310, doi: 10.1109/JSTQE.2014.2341562.

[4] R. J. Walker, J. A. Richardson, and R. K. Henderson, "A 128 $\times$ 96 pixel event-driven phase-domain $\Delta\Sigma$-based fully digital 3D camera in 0.13 μm CMOS imaging technology," in *Proc. IEEE Int. Solid-State Circuits Conf.*, 2011, pp. 410–412, doi: 10.1109/ISSCC.2011.5746374.

[5] S. Jahromi, J. Jansson, P. Keränen, and J. Kostamovaara, "A 32 $\times$ 128 SPAD-257 TDC receiver IC for pulsed TOF solid-state 3-D imaging," *IEEE J. Solid-State Circuits*, vol. 55, no. 7, pp. 1960–1970, Jul. 2020, doi: 10.1109/JSSC.2020.2970704.

[6] D. Morrison, S. Kennedy, D. Delic, M. R. Yuce, and J.-M. Redouté, "A 64 $\times$ 64 SPAD flash LIDAR sensor using a triple integration timing technique with 1.95 mm depth resolution," *IEEE Sensors J.*, vol. 21, no. 10, pp. 11361–11373, May 2021, doi: 10.1109/JSEN.2020.3030788.

[7] B. Park *et al.*, "A 64 $\times$ 64 SPAD-based indirect time-of-flight image sensor with 2-tap analog pulse counters," *IEEE J. Solid-State Circuits*, vol. 56, no. 10, pp. 2956–2967, Oct. 2021, doi: 10.1109/JSSC.2021.3094524.

[8] V. Sesta, K. Pasquinelli, R. Federico, F. Zappa, and F. Villa, "Range-finding SPAD array with smart laser-spot tracking and TDC sharing for background suppression," *IEEE Open J. Solid-State Circuits Soc.*, vol. 2, pp. 26–37, 2021, doi: 10.1109/OJSSCS.2021.3116920.

[9] O. Kumagai *et al.*, "7.3 A 189 $\times$ 600 back-illuminated stacked SPAD direct time-of-flight depth sensor for automotive LiDAR systems," in *Proc. IEEE Int. Solid- State Circuits Conf.*, 2021, pp. 110–112, doi: 10.1109/ISSCC42613.2021.9365961.

[10] F. Martin *et al.*, "An all-in-one 64-zone SPAD-based direct-time-of-flight ranging sensor with embedded illumination," in *Proc. IEEE Sensors*, 2021, pp. 1–4, doi: 10.1109/SENSORS47087.2021.9639840.

[11] R. Enne, B. Steindl, M. Hofbauer, and H. Zimmermann, "Fast cascoded quenching circuit for decreasing afterpulsing effects in 0.35-μm CMOS," *IEEE Solid-State Circuits Lett.*, vol. 1, no. 3, pp. 62–65, Mar. 2018, doi: 10.1109/LSSC.2018.2827881.

[12] H. Zimmermann *et al.*, "Integrated fiber optical receiver reducing the gap to the quantum limit," *Sci. Rep.*, vol. 7, pp. 1–2, 2017. [Online]. Available: https://doi.org/10.1038/s41598-017-02870-2

[13] K. Oberhauser, G. Zach, A. Nemecek, and H. Zimmermann, "Monolythically integrated optical distance measurement sensor with double-cathode photodetector," in *Proc. IEEE Instrum. Meas. Technol. Conf.*, 2007, pp. 1–4, doi: 10.1109/IMTC.2007.379083.